Phase-field model of eutectic growth

Alain Karma
Physics Department, Northeastern University, Boston, Massachusetts 02115
(Received 5 August 1993)

A phase-field model which describes the solidification of a binary eutectic alloy with a simple symmetric phase diagram is introduced and the sharp-interface limit of this model is explored both analytically and numerically.

PACS number(s): 61.50.Cj, 05.70.Ln, 64.70.Dv, 81.30.Fb

I. INTRODUCTION

In recent years, there has been a revival in the idea of using phase-field models as a numerical tool to study the formation of solidification patterns. These models circumvent the complications associated with sharp-interface formulations and have the advantage of handling naturally complex geometries. So far, phase-field models have been introduced to describe the solidification of pure materials [1–5] and two-phase binary alloys [6, 7], the dendritic growth of a pure substance having been the main focus of numerical studies [8, 9]. The aim of this paper is to extend the phase-field approach to model the solidification of eutectic binary alloys. Due to the presence of triple points (three-phase junctions), modeling this system has remained a difficult numerical challenge despite some successes with random-walk-based algorithms [10, 11]. A phase-field approach seems worth exploring for this problem since it handles automatically the motion of these points.

We construct the simplest possible model corresponding to an alloy with a symmetric phase diagram and with solid phases of identical physical properties. More elaborate models for specific alloys with different phase diagrams could, in principle, be constructed as an extension of the one considered here. We then perform a mathematical reduction of the phase-field equations to the classic sharp interface formulation of eutectic growth in the limit where the interface is assumed to be in local thermodynamic equilibrium (LTE) and the kinetic undercooling can be neglected. In fact, we show that for a specific choice of scaling of parameters of the model, this assumption is always valid in the limit where the scale of the eutectic pattern is large compared to the width of the rough solid-liquid interface. This permits a direct comparison of the two formulations, phase-field and sharp interface, which is conducted in the context of steady-state lamellar eutectic growth.

II. MODEL

In this section, the model is first presented for isothermal solidification conditions. Direct extensions to non-isothermal conditions and directional solidification are described at the end of this section.

A. Free energy

A phase-field formulation of eutectic growth requires a minimum of two order parameters: a nonconserved order parameter, denoted here by $u(\mathbf{r},t)$, to distinguish between solid and liquid, and the alloy composition $C(\mathbf{r},t)$. It is useful to define the composition field $c(\mathbf{r},t) \equiv C_E - C(\mathbf{r},t)$ which measures the departure from the eutectic composition C_E. The first necessary step is to construct a free-energy functional $\mathcal{F}(u,c,T)$ for the system which can be chosen to have the general form:

$$\mathcal{F}(u,c,T) = \int d\mathbf{r}\left[\frac{\zeta_c^2}{2}(\nabla c)^2 + \frac{\zeta_u^2}{2}(\nabla u)^2 + f(u,c,T)\right], \tag{1}$$

where T is the temperature and $f(u,c,T)$ represents the bulk free energy. To select the form of the latter we simply expand $f(u,c,T)$ in a power series in u and c and only retain the lowest-order coupling between u and c which is consistent with the symmetries imposed by the phase diagram and the nature of the phases. A symmetric phase diagram imposes $f(u,c,T)$ to be invariant under the transformation $c \to -c$, which in turn imposes that the lowest-order coupling between u and c be proportional to c^2. In addition, the requirement that the free energies of the solid and liquid phases have different composition dependence (i.e., a double-well function for the solid and a single-well function for the liquid) imposes that the same coupling term must also be odd in u and, hence, proportional to uc^2. With this in mind, we obtain the simple form

$$f(u,c,T) = -\frac{u^2}{2} + \frac{u^4}{4} + \frac{c^4}{4} + \frac{uc^2}{2} - [T - T_E + \Delta T^*]\,u, \tag{2}$$

where ΔT^* is a constant undercooling parameter which is uniquely determined by the condition that all three phases have the same bulk free energy at the eutectic temperature $T = T_E$. This undercooling differs from the undercooling $\Delta T \equiv T_E - T$ which is the main control parameter for isothermal growth. For simplicity, both f and T are chosen to be dimensionless here. This avoids having to carry extra dimensional constants which can

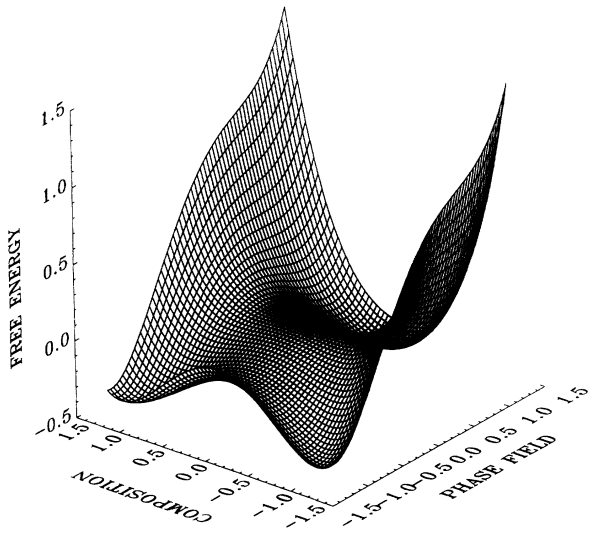

FIG. 1. Free-energy surface of the model at the eutectic temperature $f(u, c, T_E)$.

always be scaled out in the sharp interface limit. A plot of $f(u, c, T)$ at $T = T_E$ is shown in Fig. 1. The phase-field model is then defined by the equations of motion

$$\tau_u \frac{\partial u}{\partial t} = -\frac{\delta \mathcal{F}}{\delta u}, \tag{3}$$

$$\tau_c \frac{\partial c}{\partial t} = \nabla \cdot \left(M(u) \nabla \frac{\delta \mathcal{F}}{\delta c} \right), \tag{4}$$

where $M(u)$ is a mobility which is necessary to introduce in order to account for the fact that impurity diffusion is much faster in a liquid than in a solid. Although different functional forms of $M(u)$ are possible, we have chosen here the simple form

$$M(u) = \left[\frac{u - u_S^E}{u_L^E - u_S^E} \right]^2 . \tag{5}$$

With this choice, $M(u)$ is unity in the liquid and vanishes in the solid to leading order in ΔT; u_L^E and u_S^E, to be defined below, denote the stationary values of u in the liquid and solid at $T = T_E$.

Two formal connections to previous models are worth mentioning. First, if c is treated as a constant, Eq. (3) reduces to the standard phase-field model of a pure substance [2]. Second, aside from the specific choice of mobility, Eq. (4) reduces to the Cahn-Hilliard [12] equation in the solid where u approaches a negative constant ($u = u_S^E < 0$).

B. Phase diagram

To construct the phase diagram corresponding to our model, we first define the "composition-dependent" bulk free energies, $f_S(c, T)$ and $f_L(c, T)$, for the solid and the liquid, respectively. We then apply the standard common tangent construction to calculate the equilibrium compositions in the three phases as a function of temperature. The bulk free energies are defined as follows. In the bulk solid and liquid, u must be stationary which imposes the constraint

$$\frac{\partial f(u, c, T)}{\partial u} = u^3 - u + \frac{c^2}{2} - [T - T_E + \Delta T^*] = 0. \tag{6}$$

This cubic equation has three roots. The lowest root corresponds to the solid and the largest root to the liquid. These roots define two functions, $u_S(c, T) < 0$ and $u_L(c, T) > 0$. The composition-dependent bulk free energies are then defined by the relation

$$f_\nu(c, T) \equiv f(u_\nu(c, T), c, T) \quad ; \quad \nu = S, L \tag{7}$$

where $f_S(c, T)$ and $f_L(c, T)$ are, respectively, a double-well function and a single-well function of c (as can be seen in Fig. 1 by looking at constant u sections of the free-energy surface). This structure imposes that there exists, in general, two common tangents between $f_S(c, T)$ and $f_L(c, T)$ which define four compositions denoted by $c_\nu^\mu(T)$ where the subscript ($\nu = S, L$) refers to the solid and liquid phases and the superscript ($\mu = \alpha, \beta$) to the α and β phases. The symmetry of the present phase diagram imposes that $c_\nu^\alpha(T) = -c_\nu^\beta(T)$. These functions define the (α,β) solidus and liquidus of the phase diagram shown in Fig. 2. The latter become metastable for $T < T_E$ (as indicated by the dashed lines). For $T < T_E$, the equilibrium compositions in the thermodynamically stable solid α and β phases, corresponding to the two legs of the phase diagram, are defined by the common tangent of the two wells of $f_S(c, T)$. Finally, the constraint $c_L^\alpha(T_E) = c_L^\beta(T_E)$ fixes the value of the constant ΔT^*. For what follows, it is useful to define the constants $c_\alpha = c_S^\alpha(T_E)$, $c_\beta = c_S^\beta(T_E)$, and $c_E = c_L^\alpha(T_E) = c_L^\beta(T_E)$, to denote the equilibrium compositions of the three phases (solid α, solid β, and liquid), at $T = T_E$ and

$$m_L \equiv \left| \frac{c_L^\nu(T)}{dT} \right|_{T=T_E}^{-1} , \quad \nu = \alpha, \beta \tag{8}$$

to denote the slope of the equilibrium liquidus. In

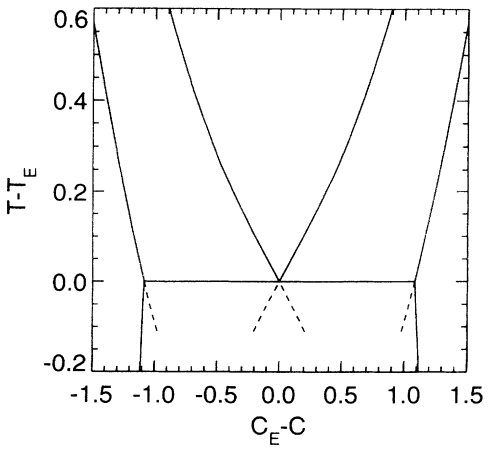

FIG. 2. Equilibrium phase diagram of the model.

TABLE I. Parameters used to construct the phase diagram. See text for details.

ΔT^*	0.140
u_S^E	−1.175
u_L^E	1.064
c_α	−1.084
c_β	1.084
c_E	0
m_L	0.515

terms of the above, the constants appearing in the definition of the mobility [Eq. (5)] are defined by $u_\nu^E = u_\nu(c_E, T_E)(\nu = S, L)$ with u_S^E having the same value in both the solid α and β phases. Numerical values of the parameters are summarized in Table I.

One limitation of the present model, already apparent in Fig. 2, is that the solidus and liquidus do not intersect at some higher temperature T_M which should, in principle, correspond to the melting temperature of the pure material. Hence, this model cannot be used to describe the evolution of solidification microstructures all the way to the dilute limit. Nonetheless, it permits the investigation of a range of off-eutectic composition (for which it is mainly intended).

C. Sharp-interface limit

To reduce the phase-field Eqs. (3) and (4) to the classical free-boundary formulation of eutectic growth, we restrict our attention to a limit in which the interface is assumed to be in LTE. Simple scaling arguments can be used to show that this is indeed the right limit to consider for eutectic growth with the choice of parameter scaling $\zeta_u \sim \zeta_c$ and $\tau_u \sim \tau_c$. To simplify the discussion, let us consider the case where $\zeta_u = \zeta_c = \zeta$ and $\tau_u = \tau_c = \tau$. We also write an expression for the solute diffusivity in the liquid which we need below. The latter can be obtained from Eq. (4) which becomes a simple diffusion equation away from the interface where concentration gradients are weak. It takes the form

$$D_L = \frac{\zeta^2 M(u)}{\tau}\frac{\partial^2 f}{\partial c^2} \cong \frac{\zeta^2}{\tau}[u_L^E + 3c^2], \tag{9}$$

where the second equality on the right-hand side of Eq. (9) is strictly valid for $\Delta T \ll 1$. We note in passing that the above diffusivity has a weak quadratic dependence on c which could, in principle, be removed by choosing a more complex form of mobility which depends on both u and c. In the neighborhood of the eutectic composition, it takes on the nearly constant value $D_L \cong u_L\zeta^2/\tau$.

We are looking for a condition which tells us when the interface can be assumed to be in LTE or, equivalently, when the kinetic undercooling ΔT_K is small compared to ΔT. On purely dimensional grounds, it is easy to see from Eqs. (3) and (4) that the former must scale as

$$\Delta T_K \sim \frac{v\tau}{\zeta}, \tag{10}$$

where v is the growth rate of the interface. The desired condition is then obtained by realizing that, for a eutectic interface, the maximum growth rate (which sets the velocity scale in the problem) must behave as

$$v \sim \frac{D_L}{\zeta}\Delta T^2, \tag{11}$$

for small ΔT. Equation (11) is essentially the classic result of the Jackson-Hunt [13] analysis transcribed in terms of the present parameters. It follows immediately that the interface can be assumed to be in LTE when $\Delta T_K \ll \Delta T$ which, using Eqs. (9)–(11), implies that $\Delta T \ll 1$. This, in turn, implies that the eutectic spacing $\lambda \sim \zeta/\Delta T$ corresponding to the maximum growth rate—which in turn sets the scale of the microstructure—satisfies the condition

$$\lambda \gg \zeta. \tag{12}$$

The interesting point here is that this last condition is exactly what defines the sharp-interface limit of the phase-field model. We therefore arrive at the conclusion that for $\zeta_c \sim \zeta_u$ and $\tau_c \sim \tau_u$ the approximation of LTE is always valid in the sharp-interface limit of the present model where the eutectic interface is curved on a scale larger than its width ζ. Following this choice of scaling, the only additional parameters which need to be calculated to completely specify the sharp-interface limit of the model are the three surface energies $\gamma_{\alpha L} = \gamma_{\beta L}$ and $\gamma_{\alpha\beta}$ at the eutectic point. With our present parametrization, these have unit of length and are defined by the relation

$$\gamma_{\mu\nu} = \int dx\left[\frac{\zeta_c^2}{2}(\nabla c_{\mu\nu})^2 + \frac{\zeta_u^2}{2}(\nabla u_{\mu\nu})^2 + f(u_{\mu\nu}, c_{\mu\nu}, T_E) - f_B^E\right], \tag{13}$$

where f_B^E denotes the equilibrium bulk free energy which is equal in all three phases at the eutectic temperature and $u_{\mu\nu}$ and $c_{\mu\nu}$ are the one-dimensional stationary profiles connecting the μ and ν phase. Following Eqs. (3) and (4), these profiles can be obtained numerically by solving the system of two coupled one-dimensional ordinary differential equations,

$$\zeta_u^2\frac{d^2u_{\mu\nu}}{dx^2} = -u_{\mu\nu} + u_{\mu\nu}^3 + c_{\mu\nu}^2/2 - \Delta T^*, \tag{14}$$

$$\zeta_c^2\frac{d^2c_{\mu\nu}}{dx^2} = c_{\mu\nu}^3 + u_{\mu\nu}c_{\mu\nu}, \tag{15}$$

subject to the boundary condition that $u_{\mu\nu}$ and $c_{\mu\nu}$ approach their stationary equilibrium values in the μ and ν phase for $x \to -\infty$ and $x \to +\infty$, respectively. Numerical values of $\gamma_{\mu\nu}$ calculated using Eqs. (13)–(15) for the special case where $\zeta_u = \zeta_c = \zeta$ are given in Table II. The requirement that the $\mathcal{F}$ be stationary under an arbitrary deformation of the interface leads to the Gibbs-Thomson conditions

$$m_L c = \Delta T - \Gamma\kappa, \quad \alpha L \text{ interface} \tag{16}$$

$$m_L c = -\Delta T + \Gamma\kappa, \quad \beta L \text{ interface} \tag{17}$$

where $\kappa \ll \zeta^{-1}$ and

TABLE II. Parameters used for the sharp-interface limit of the model. See text for details. Values are for $\zeta_c = \zeta_u = \zeta$.

$\gamma_{\nu L}/\zeta$	1.47[a]
$\gamma_{\alpha\beta}/\zeta$	1.10
Γ/ζ	0.656
θ	22°
$D_L\tau/\zeta^2$	1.064[b]

[a] $\nu = \alpha, \beta$.
[b] Strictly valid for $c \ll 1$ [see Eq. (9)].

$$\Gamma \equiv \frac{\gamma_{\nu L}}{u_L^E - u_S^E}\ , \quad \nu = \alpha, \beta. \tag{18}$$

Mass conservation at the interface requires that

$$c_\nu\, v_n \ = \ D_L\, \hat{\mathbf{n}} \cdot \nabla c\ , \quad \nu = \alpha, \beta \tag{19}$$

where v_n denotes the normal velocity of the interface. Diffusion in the liquid is governed by Eq. (4) which, away from the boundary, reduces to the usual diffusion equation

$$\frac{\partial c}{\partial t} \ = \ D_L\, \Delta c. \tag{20}$$

Finally, the condition of mechanical equilibrium at the interface requires that

$$\gamma_{\alpha L}\hat{\mathbf{t}}_{\alpha L} + \gamma_{\beta L}\hat{\mathbf{t}}_{\beta L} + \gamma_{\alpha\beta}\hat{\mathbf{t}}_{\alpha\beta} = 0, \tag{21}$$

where $\hat{\mathbf{t}}_{\mu\nu}$ denotes the tangent vector to the μ–ν interface pointing outwards from the triple point. Equations (16)–(21) together with the boundary condition

$$c = c_\infty \qquad \text{for} \qquad z = \infty \tag{22}$$

completely define the sharp-interface limit, $\kappa \ll \zeta^{-1}$, of the model.

D. Extension to nonisothermal conditions

The present model can be straightforwardly extended to describe nonisothermal solidification conditions by supplementing Eqs. (3) and (4) with the equation for the temperature field

$$\frac{\partial T}{\partial t} \ = \ D_T \Delta T + \left[\frac{L}{u_L^E - u_S^E}\right] \frac{\partial u}{\partial t}, \tag{23}$$

where L is the latent heat of melting assumed to be equal for both α and β phases, and D_T is the thermal diffusivity assumed to be equal in all three phases.

In practice, one of the most often encountered nonisothermal condition is directional solidification where a sample is pulled in a temperature gradient at a constant speed V. Since $D_T \gg D_L$, latent heat diffusion is negligible at low enough velocity and the temperature field can be assumed to have the usual form

$$T \ = \ T_E + Gz, \tag{24}$$

where z is a coordinate parallel to the temperature gradient which is fixed in the laboratory frame and moving at velocity V in the frame of the sample being pulled. Directional solidification is therefore simply described by transforming the phase-field equations to this moving frame. Equations (3) and (4) become

$$\tau_u \frac{\partial u}{\partial t} = \tau_u V \frac{\partial u}{\partial z} - \frac{\delta \mathcal{F}}{\delta u}, \tag{25}$$

$$\tau_c \frac{\partial c}{\partial t} = \tau_c V \frac{\partial c}{\partial z} + \nabla \cdot \left(M(u) \nabla \frac{\delta \mathcal{F}}{\delta c} \right), \tag{26}$$

where T in Eq. (2) is now given by Eq. (24). Correspondingly, in the sharp-interface limit, the diffusion Eq. (20) is transformed to

$$\frac{\partial c}{\partial t} \ = \ V \frac{\partial c}{\partial z} + D_L\, \Delta c, \tag{27}$$

and the Gibs-Thomson conditions become

$$m_L\, c = -G\xi - \Gamma\, \kappa\ , \qquad \alpha\text{-}L \text{ interface} \tag{28}$$

$$m_L\, c = G\xi + \Gamma\, \kappa\ , \qquad \beta\text{-}L \text{ interface} \tag{29}$$

where ξ denotes the vertical displacement of the interface parallel to the z axis ($\xi = 0$ corresponding to an interface at the eutectic temperature).

III. NUMERICAL SIMULATIONS

In this section we present the results of numerical simulations of the phase-field equations. These simulations are mainly intended to demonstrate that the model actually produces eutectic structures which are in good agreement with those expected from the sharp-interface limit derived above.

For this purpose, we consider a spatially periodic steady-state lamellar structure formed by directional solidification of an alloy of exactly eutectic composition ($c_\infty = c_E = 0$). For this structure, the Jackson-Hunt theory [13] leads to the prediction

$$\Delta T(\lambda) \ = \ V \lambda \frac{2\, P\, m_L\, [c_\beta - c_\alpha]}{D_L} \ + \ \frac{4\, \Gamma \sin\theta}{\lambda}, \tag{30}$$

where λ is the lamellar spacing, $\Delta T = T_E - T_I$ is the interfacial undercooling, T_I is the interface temperature which can be assumed to be constant for sufficiently small G, $P = 0.03383$ is a numerical constant, and

$$\theta \ = \ \sin^{-1}\left[\frac{\gamma_{\alpha\beta}}{2\gamma_{\nu L}}\right] \quad , \quad \nu = \alpha, \beta \tag{31}$$

is the angle between a horizontal x axis, which lies parallel to the eutectic front, and an axis tangent to the solid-liquid interface at the triple point.

Numerical simulations of Eqs. (25) and (26) were performed on a two-dimensional lattice of sides $L_x = N_x h$ and $L_z = N_z h$ with periodic and no flux boundary conditions in the horizontal and vertical directions, respectively. The origin of the z axis was chosen such that Eq. (24) takes the form $T = T_E + G(z - L_z/2)$ with $z = jh$ ($j = [1, N_z]$). For simplicity, the parameters $\zeta_c = \zeta_u = \zeta$ and $\tau_u = \tau_c = \tau$ were chosen. The value $G = 2.85 \times 10^{-3}\, \zeta^{-1}$ was used in all simulations. A fi-

nite difference representation of spatial derivatives with $h = \zeta$ was used in conjunction with a simple Euler time-stepping scheme with $\Delta t = 0.015\ \tau$. These values of h and Δt were found to provide a good compromise between numerical accuracy which requires h to be small and computational efficiency which requires Δt to be large. In particular, since numerical stability imposes the condition $\Delta t < A\ h^4$, where A is a constant of order unity, smaller values of h were found to require too small a value of Δt to allow a systematic numerical study. In addition, larger values of h led to grid anisotropies that were too large, the number of points necessary to resolve the spatially diffuse interfacial region being insufficient. We also explored the possibility of using an implicit scheme, which allows to take larger time steps for a given h, but the extra computational cost involved with this scheme did not seem to outweigh the numerical efficiency of the explicit scheme which lends itself naturally to parallel programming on the Cray 2 supercomputer used in this investigation.

The stationary interface profile resulting from a simulation on a 160×160 lattice with $V = 0$ is shown in Fig. 3 on a one-to-one scale. The solid-liquid and α-β interfaces are represented, respectively, by the $u = 0$ and ($c = 0$, $u < 0$) contours. They correspond to the expected stationary shape of a lamellar structure consisting of two circular arcs which join the α-β interfaces at triple points. The measured angle at the triple point has a value $\theta \approx 18° \pm 2°$ which is in relatively good quantitative agreement with the value $\theta = 22°$ predicted by Eq. (31) in the sharp-interface limit with the values of Table II.

A series of simulations intended to measure the $\Delta T(\lambda)$ curve was performed for a pulling speed $V = 0.01\ \zeta/\tau$. The lamellar spacing $\lambda = N_x h$ was varied between between 18 and 80 ζ, with the vertical dimension of the lattice $L_z = 100\ \zeta$ held fixed. Simulations were ran long enough for the interface to reach a steady state. The undercooling was measured using the relationship $\Delta T(\lambda) = -G\bar{\xi}$ where $\bar{\xi}$ denotes the average vertical position of the solid-liquid interface. As shown in Fig. 4, the measured $\Delta T(\lambda)$ curve was found to be in relatively good quantitative agreement with the curve predicted by the Jackson-Hunt theory [Eq. (30)] using the parameters of Tables I and II. The interface shapes corresponding to three different wavelengths along this curve are displayed in Fig. 5.

It should be noted that the quantitative discrepancy between the two curves in Fig. 4 may be due both to

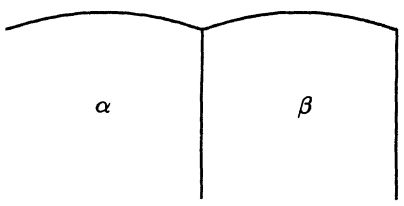

FIG. 3. Stationary eutectic profile obtained from simulation on a 160×160 lattice with $V = 0$.

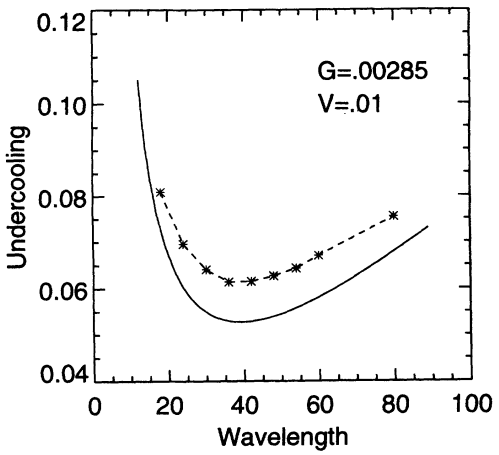

FIG. 4. Undercooling vs wavelength curve: Jackson-Hunt theory corresponding to Eq. (30) (solid line) and results of simulations (stars and dashed line). The wavelength is measured in units of ζ, G in units of ζ^{-1}, and V in units of ζ/τ.

the limitation of the Jackson-Hunt theory which only becomes exact in the limit of very small angle ($\theta \to 0$), and to the fact that the sharp-interface limit is likely not to be completely reached with the lattice sizes employed here. To highlight the difficulty encountered in studying larger lattices, it is useful to give an estimation of the required number of floating-point operations, N, necessary to simulate the growth of one eutectic spacing at minimum undercooling (i.e., $L_x = \lambda_m$). This number scales as $N = N_0(\lambda_m/\zeta)(L_z/\zeta)(\tau/\Delta t)(t/\tau)$ where $N_0 \sim 10^2$ is a constant prefactor independent of the lattice size and t is the total simulation time. A good estimate of the latter is the time it takes for the interface to move a distance comparable to λ_m which scales as $t \sim \lambda_m/V$. In addition, the fact that for an alloy of eutectic composition $c(x, z)$ decays exponentially in z over a length proportional to λ_m implies that $L_z \sim \lambda_m$ (note that at off-eutectic composition this decay length is proportional to the diffusion length which requires $L_z \sim D_L/V$). Finally, using the

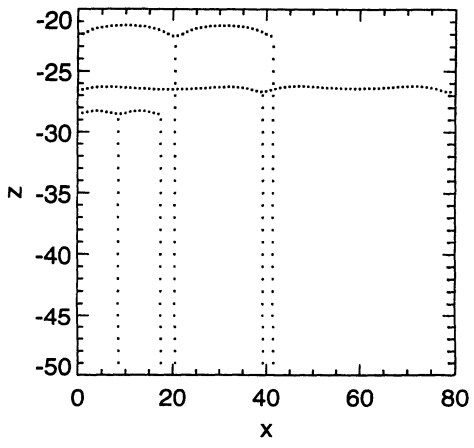

FIG. 5. Eutectic profiles corresponding to Fig. 4 for $\lambda/\zeta = 18, 42$, and 80; x and z are measured in units of ζ.

fact that $V \sim D_L\zeta/\lambda_m^2 \sim (\zeta/\tau)(\zeta/\lambda_m)^2$ at minimum undercooling together with the above scalings, we obtain the estimate

$$N = N_0 \left(\frac{\tau}{\Delta t}\right)\left(\frac{\lambda_m}{\zeta}\right)^5. \quad (32)$$

The fifth power in Eq. (32) explains why it becomes quickly prohibitive from a computational standpoint to simulate eutectic structures with a ratio λ_m/ζ greater than the ratio of about 40 used here. For example, to generate the data of Fig. 4 with λ_m doubled (i.e., V four times smaller) would require a computational effort 32 times larger. What seems encouraging, however, is that already with the present ratio, the model generates an undercooling-wavelength curve which is relatively close from the one expected from the sharp-interface limit.

IV. CONCLUSION

In conclusion, we have presented a phase-field model that can describe the solidification (both isothermal and nonisothermal) of a eutectic binary alloy with a simple symmetric phase diagram. We have analyzed the sharp-interface limit of this model with a specific choice of parameter scaling $\zeta_c \sim \zeta_u$ and $\tau_c \sim \tau_u$. With this choice of scaling, the limit where the lamellar spacing is much larger than the interface width corresponds precisely to the limit of LTE where the interfacial kinetic undercooling is much smaller than the overall interfacial undercooling induced by the combined effects of surface tension and solute diffusion. Hence, with this choice of scaling, there is a one-to-one correspondance between the phase-field model and the classic sharp interface formulation of eutectic growth *without* nonequilibrium corrections. We have actually demonstrated numerically in this paper that the phase-field equations generate steady-state lamellar structures which are in relatively good quantitative agreement with those expected from the sharp interface formulation using computationally tractable lattice sizes.

In the future, it might be worth exploring different parameter scalings of the present model and, in particular, the one corresponding to the limit $\zeta_u \ll \zeta_c$ which has been investigated previously for simple binary alloys in Ref. [7]. With this scaling, it should be possible to describe situations where, simultaneously, the lamellar spacing is much larger than the interface width and nonequilibrium effects such as solute trapping are important, as we expect to be the case for many rapidly solidified eutectic alloys.

ACKNOWLEDGMENTS

This research was supported by U.S. DOE Grant No. DE-FG02-92ER45471. The allocation of supercomputer time at NERSC is acknowledged.

[1] G. J. Fix, in *Free Boundary Problems: Theory and Applications, Vol. II*, edited by A. Fasano and M. Primicerio (Piman, Boston, 1983), p. 580.
[2] J. S. Langer, in *Directions in Condensed Matter* (World Scientific, Singapore, 1986), p. 164.
[3] J. B. Collins and H. Levine, Phys. Rev. B **31**, 6119 (1985).
[4] J. Deutsch (unpublished).
[5] G. Caginalp, Phys. Rev. A **39**, 5887 (1989).
[6] A. A. Wheeler, W. J. Boettinger, and G. B. McFadden, Phys. Rev. A **45**, 7424 (1992).
[7] A. A. Wheeler, W. J. Boettinger, and G. B. McFadden, Phys. Rev. E **47**, 1893 (1993).
[8] A. A. Wheeler, B. T. Murray, and R. J. Schaefer, Physica D **66**, 243 (1993).
[9] R. Kobayashi, Bull. Jpn. Soc. Ind. Appl. Math. **1**, 22 (1991); videotape in *Computational Crystal Grower Workshop*, AMS Selected Lectures in Mathematics, edited by Jean Taylor (American Mathematic Society, Providence, RI, 1992).
[10] A. Karma, Phys. Rev. Lett. **59**, 71 (1987); videotape in *Computational Crystal Grower Workshop*, AMS Selected Lectures in Mathematics, edited by Jean Taylor (American Mathematical Society, Providence, RI, 1992).
[11] R.-F. Xiao, J. I. D. Alexander, and F. Rosenberger, Phys. Rev. A **45**, R571 (1992).
[12] J. W. Cahn and J. E. Hilliard, J. Chem. Phys. **28**, 258 (1958).
[13] K. A. Jackson and J. D. Hunt, Trans. Metall. Soc. AIME **236**, 1129 (1966).

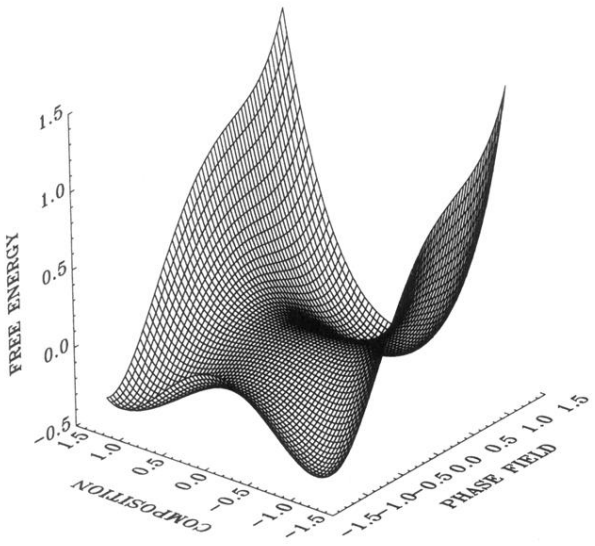

FIG. 1. Free-energy surface of the model at the eutectic temperature $f(u, c, T_E)$.